

Uniformity of cylindrical imploding underwater shockwaves at very small radii

D. Yanuka,¹ A. Rososhek,¹ S. N. Bland,² and Ya. E. Krasik¹

¹Physics Department, Technion, Haifa 32000, Israel

²Institute of Shock Physics, Imperial College London, London SW7 2BW, United Kingdom

(Received 18 September 2017; accepted 6 November 2017; published online 21 November 2017)

We compare the convergent shockwaves generated from underwater, cylindrical arrays of copper wire exploded by multiple kilo-ampere current pulses on nanosecond and microsecond scales. In both cases, the pulsed power devices used for the experiments had the same stored energy (~ 500 J) and the wire mass was adjusted to optimize energy transfer to the shockwave. Laser backlit framing images of the shock front were achieved down to the radius of $30\ \mu\text{m}$. It was found that even in the case of initial azimuthal non-symmetry, the shock wave self-repairs in the final stages of its motion, leading to a highly uniform implosion. In both these and previous experiments, interference fringes have been observed in streak and framing images as the shockwave approached the axis. We have been able to accurately model the origin of the fringes, which is due to the propagation of the laser beam diffracting off the uniform converging shock front. The dynamics of the shockwave and its uniformity at small radii indicate that even with only 500 J stored energies, this technique should produce pressures above 10^{10} Pa on the axis, with temperatures and densities ideal for warm dense matter research. *Published by AIP Publishing.* <https://doi.org/10.1063/1.5005174>

The subject of Warm Dense Matter (WDM) has been under intense investigation¹ for several decades due to its importance in many fields of research such as Equations Of State (EOS), conductivity models, astrophysics, geophysics, and inertial confinement fusion.^{2–4} There are several methods for obtaining WDM, which include chemical and nuclear explosions,⁵ z-pinchs,⁶ high-power lasers,^{7,8} light-gas guns,⁹ and high-energy (GeV range) ion beams.¹⁰ These methods require special safety measures, large and expensive facilities, and stored energies above 10^5 J.

The results of recent studies indicate that WDM with pressures above 100 GPa can be obtained using strong converging Strong Shock Waves (SSWs) generated by underwater electrical explosions of either cylindrical or spherical wire arrays.^{11,12} Different methods (damage of different targets, spectroscopy of the obtained water plasma created by the convergence of the SSW) were applied to determine the water parameters in the vicinity of implosion.^{13–15} Also, the SSW's time-of-flight to the axis (cylindrical wire array) or origin (spherical wire array) of implosion leading to intense light emission from compressed and heated water at those locations was used for comparison with the results of one dimensional (1D) and two dimensional (2D) Hydrodynamic (HD) simulations, coupled with the EOS of water and copper.¹⁶ In these simulations, which considered symmetrical SSW convergence, only the energy deposition rate into the wires, calculated using the experimentally obtained resistive voltage and discharge current waveforms, was an input parameter.

In the 1D HD simulations, a symmetrically propagating SSW is assumed, and in the 2D HD simulations, possible SSW instabilities are not typically taken into account. However, the issue of instabilities, which could lead to a non-uniform azimuthal implosion of the SSW, is of crucial importance for the validity of these simulations and consequently

for the values of the water parameters in the vicinity of implosion. Despite the comprehensive research devoted to converging shock wave instabilities,^{17–19} there is no complete understanding regarding the range of applicabilities and the correctness of the existing models and simulations.²⁰ Shadowgraph images of converging cylindrical SSWs generated by underwater electrical explosions of wire arrays obtained in experiments carried out in Technion and Imperial College London showed a near circular shape of the SSW's front down to a radius of $100\ \mu\text{m}$.^{11,21,22}

In this paper, the results of cylindrical SSW convergence below a radius of $100\ \mu\text{m}$ are described and analyzed. In addition, beam propagation method (BPM) simulations have been applied to study the propagation of a laser beam that is used to backlight framing and streak images of the implosion. The results of these simulations showed interference patterns which almost perfectly fit the inference patterns obtained in these and previous experiments.

The research was carried out using nanosecond- and microsecond-scale pulse generators. The nanosecond-scale generator is based on the discharge of a water forming line charged by a Marx generator.²³ This generator, at ± 33 kV charging voltage of the Marx generator (stored energy of ~ 500 J), produces an ~ 80 ns duration pulse at a $1.5\ \Omega$ matched resistive load with voltage and current amplitudes of 120 kV and 50 kA, respectively. The microsecond-scale generator consists of 4 low-inductance, high-voltage capacitors of $0.22\ \mu\text{F}$ each, connected in parallel, and a triggered spark gap switch. This generator charged up to 35 kV (stored energy of ~ 540 J) produces a pulse with a quarter of a period of $\sim 1\ \mu\text{s}$ and an amplitude of 35 kA at a short-circuit load placed instead of the wire array. Both nanosecond- and microsecond-scale generators produced at their output high voltage pulses with negative polarity. The high-current pulses produced by the nanosecond- and microsecond-scale generators were applied to cylindrical

wire arrays of 5 mm in diameter, consisting of 20 copper wires, and 3 cm in length, and each wire was $23\ \mu\text{m}$ and $50\ \mu\text{m}$ in diameter for the nanosecond and microsecond timescales, respectively. Following the action integral,²⁴ this choice of wires should correspond to the wires' explosion at ~ 0.8 of the maximal current amplitude.

The experimental setup is shown in Fig. 1 for the nanosecond timescale (the microsecond timescale setup is identical except for the generator used). A single mode 532 nm, 2.5 W, continuous wave laser (by Roithner Lasertechnik GmbH) was used for the backlighting of the converging SSWs. The laser was coupled to a single mode fiber to spatially filter the beam, removing/reducing any speckle effect in subsequent images. The output from the fiber was collimated to produce a $\sim 3\text{ mm}$ radius beam that was directed through a fused silica window into the water-filled stainless steel chamber coaxial with the wire array (see Fig. 1). An imaging lens was placed outside of the chamber to image the SSW's front using either an XXRapidFrame framing camera (Stanford Computer Optics, Germany), allowing four time-independent frames with a duration of above 1 ns, or a SC-10 streak camera (Optronis GmbH, Germany). The discharge current I through the wire was measured using a current view resistor, and the voltage drop φ across the exploding wire was measured using a capacitive voltage divider.

Typical current, resistive voltage $\varphi_r = \varphi - LdI/dt$ (L is the load's inductance), power, and deposited energy waveforms are shown in Fig. 2 for the nanosecond and microsecond-scale explosions. The deposited power and energy were calculated using the experimentally obtained current and voltage waveforms. One can see that the selection of the wires' parameters allowed us to obtain almost critically damped discharges where most of the stored energy was deposited into

the wires during $\sim 100\text{ ns}$ and $\sim 1200\text{ ns}$ in the nanosecond- and microsecond-scale explosions, respectively. The maximal current densities realized in the exploding wires were below 6000 MA/cm^2 and 1600 MA/cm^2 for the nanosecond and microsecond-scale explosions, respectively.

For each timescale, shadowgraph images of the SSW's front were obtained at low magnification ($\sim 6\text{ mm}$ in diameter) with the exploding wires included in the frame and at high magnification ($\leq 1\text{ mm}$ in diameter) to obtain only the final stages of the SSW's convergence.

Low magnification framing images from both nanosecond and microsecond-scale experiments showed that when the imploding shock front was formed from the overlapping explosions of adjacent wires, it was often not azimuthally symmetric. This can be related to a technical problem of placing the wires uniformly around on a small diameter (with an equal distance of 0.75 mm between them). An example of such initial azimuthal deformation of the shock front is shown in Fig. 3(a) where three overlapping frames obtained using the XXRapidFrame camera are shown for a microsecond timescale explosion. Typical overlapping images of a nearly circular azimuthal symmetry are shown for comparison in Figs. 3(b) and 3(c).

Experiments at high magnification were complicated by the need for extremely high accuracy in aligning the laser with the axis of the array, i.e., better than 1° alignment is needed in order to obtain images at radii below 0.1 mm ; otherwise, the perfectly cylindrical implosions are obscured and appear to be elliptical. With improvements in the alignment technique, it was found that even shockwaves that were initially highly asymmetric tended to repair themselves as they imploded towards the axis. Typical shadowgraph images of the converging SSW for nanosecond and microsecond scales

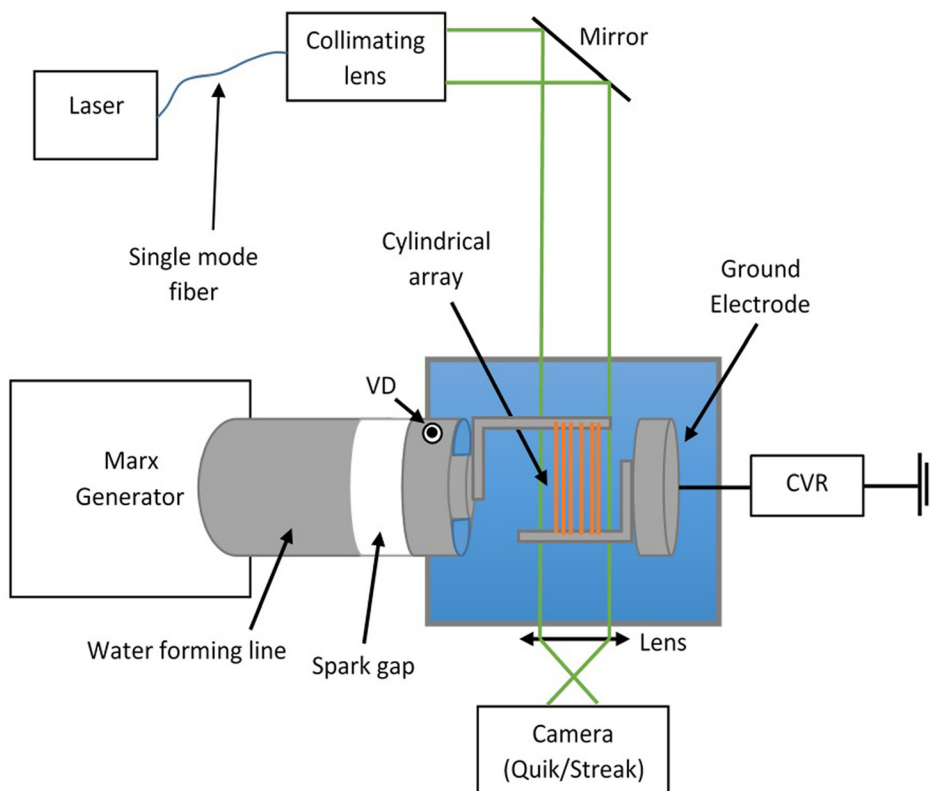


FIG. 1. Experimental setup with the nanosecond timescale generator.

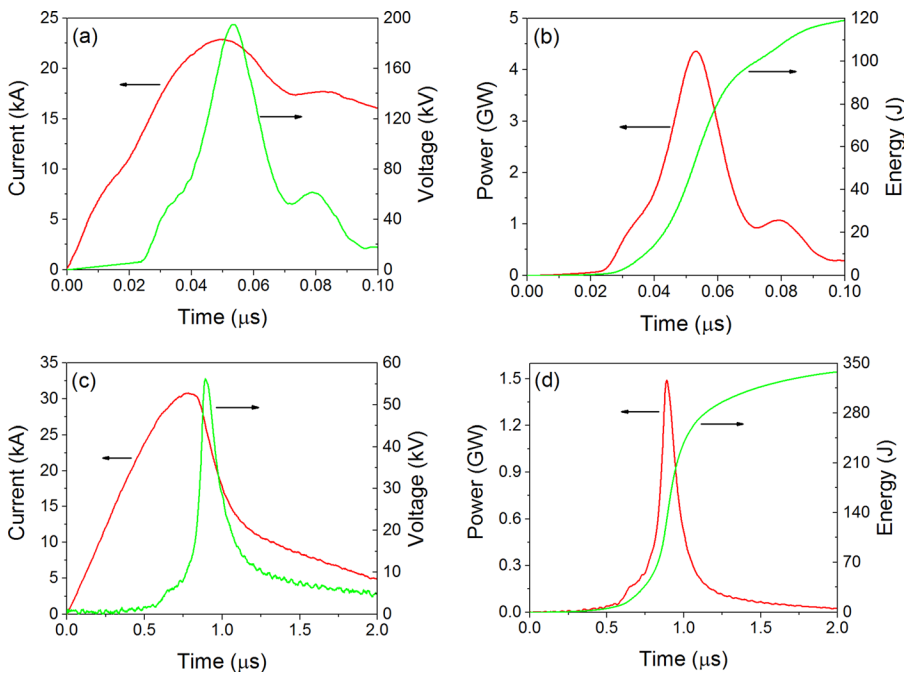


FIG. 2. Waveforms of the measured current and resistive voltage for (a) nanosecond and (c) microsecond-scale wire array explosions. Calculated power and energy for (b) nanosecond and (d) microsecond-scale wire array explosions.

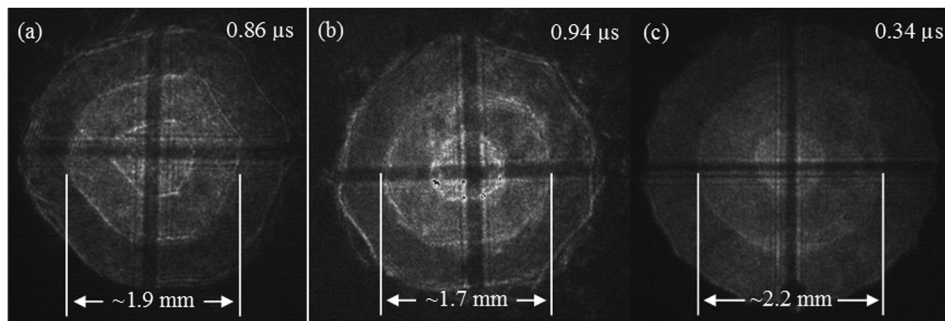


FIG. 3. Three overlapping shadowgraph images of the SSW front with (a) azimuthal non-uniformity and (b) and (c) nearly circular symmetry. (a) and (b) are for the microsecond timescale and (c) for the nanosecond timescale. The times are with respect to the beginning of the discharge current, and the time between each frame is 300 ns. Each frame duration is 2 ns. The cross in the images is because of wires placed at the front and back sides of the array for optical alignment.

are shown in Fig. 4. Here, four separate shadowgraph images are presented, obtained using the XXRapidFrame camera, for better accuracy of the SSW imaging at higher SSW velocity. One can see clearly the self-repairing nature of the SSW’s evolution especially at the final stage of implosion. In the first frame of the nanosecond timescale image [Fig. 4(a)], the radius of the SSW front is $\sim 190 \mu\text{m}$, and the front is rather azimuthally non-uniform. But the third frame [Fig. 4(c)], obtained with a delay of 50 ns with respect to the first

frame, is almost circular front. Finally, the fourth frame [Fig. 4(d)], obtained with 20 ns with respect to the third frame, showed no detectable instabilities at a radius of $\sim 30 \mu\text{m}$. Similar self-repair of the converging shock front was obtained for the microsecond timescale experiments [Figs. 4(e)–4(h)], where the shock wave’s radius is $\sim 275 \mu\text{m}$ in the first frame [Fig. 4(e)] and reaches a radius of $\sim 35 \mu\text{m}$ in the fourth frame [Fig. 4(h)] obtained with a time delay of 150 ns with respect to the first frame. Here, let us note that there

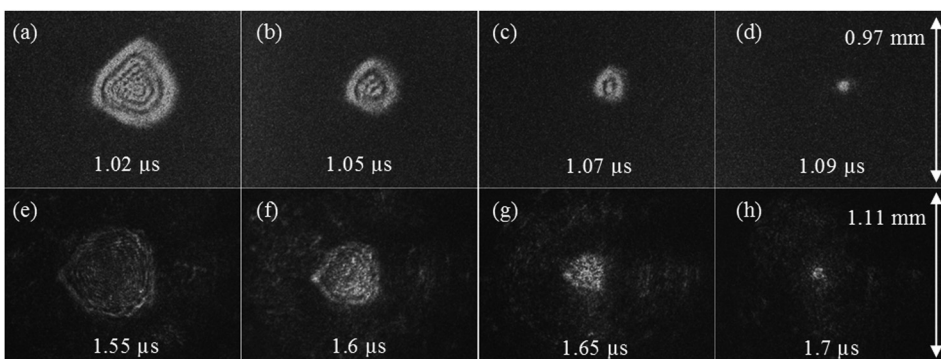


FIG. 4. Shadowgraph images of the SSWs obtained with large magnification at different times for the (a)–(d) nanosecond- and (e)–(h) microsecond-scale wire array electrical explosions. Each frame time duration is 2 ns. The times are relative to the beginning of the discharge current.

were difficulties related to obtaining shadowgraph images of the SSW at radii smaller than $30\ \mu\text{m}$. The first difficulty was in the triggering of the framing camera when the SSW arrived to a radius below $30\ \mu\text{m}$ because it takes only several nanoseconds for the SSW to arrive to the origin from that position. Also, taking shadowgraph images at radii smaller than $30\ \mu\text{m}$ becomes challenging because the shockwave begins to radiate (due to high temperature and density of water behind the shock front) and generates a plasma layer with thicknesses of several microns in front of the shockwave, thus smearing its front.

In these and previous experiments, interference fringes are clearly visible in both high magnification framing images and laser backlit streak photographs taken across the diameter of the array. To explain the fringes, a 2D fast Fourier transform-based BPM simulation²⁵ was carried out. In these simulations, the laser beam is considered as a wave propagating inside the cylinder which models the shock front. The wave propagation is governed by the Helmholtz equation in the paraxial approximation, i.e., the amplitude of the wave varies slowly outwards from the axis (along the x -axis in our case) and rapidly in the direction of propagation (along the z axis in our case). The boundary conditions are the values of the refractive index $n(x, z)$, and the initial condition is the amplitude of the wave. Because the boundary of the SSW is highly reflective, the refractive index was set to be two orders of magnitude larger at the location of the SSW and outwards than the refractive index of water inside the cylinder, which was set to 1.32. These simulations do not account for the acceleration of the SSW during its convergence towards the axis, i.e., the decrease in the cylinder's radius versus time was considered linear, which is applicable to the majority of implosion.

The plot in Fig. 5(a) represents the results of BPM simulations of the light intensity, which one can obtain in the middle of the cylinder for different SSW radii, i.e., at different times of the SSW's convergence. Experiments with the SC-10 streak camera (the width of the input slit is $0.1\ \text{mm}$, and the focus of the camera was at the middle of the array) were carried out to obtain a shadowgraph streak image of the converging SSW and compared with the simulation results. One can see a good agreement between the fringes obtained in the experiments and simulations. The slopes of the

experimental and simulated fringes are almost linear and coincide during the first $\sim 300\ \text{ns}$ and correspond to $\sim 1.75 \times 10^5\ \text{cm/s}$ of SSW velocity. Later, the slope of experimental fringes increases due to the SSW's acceleration towards the axis during the final stage of implosion. The coincidence between the simulated and experimentally obtained fringes during around $300\ \text{ns}$ of the shockwave propagation indicates an azimuthal and longitudinal uniformity of the converging shockwave. In addition, in Fig. 5(b), one can see a strong light emission which indicates high water temperature and density in the vicinity of implosion. The duration of this light emission is $\sim 100\ \text{ns}$, and the time difference between the end of the resolvable streak image of the converging SSW front and the beginning of this light emission is less than $15\ \text{ns}$. This time delay can be related to a small misalignment of the slit of the streak camera and the axis of the converging SSW. The SSW's velocity at radii below $50\ \mu\text{m}$, estimated from the streak image of the SSW, is larger than $3 \times 10^5\ \text{cm/s}$. This allows one to estimate the minimal radius where the SSW was obtained at $\sim 45\ \mu\text{m}$. Let us note that in order to obtain the SSW's convergence at smaller radii, the alignment of the optical system should be better than $1.5 \times 10^{-3}\ \text{deg}$. Thus, the BPM simulations and experimentally obtained streak shadowgraph images confirm the uniformity of the SSW convergence up to a compression factor of ~ 60 .

The present experimental results show an implosion down to at least $60\ \mu\text{m}$ in diameter. The pressure of water at that location was calculated using a 2D HD simulation coupled with EOSs of water and copper. These simulations, based on the cell-centered finite volume method and three conservation laws (mass, momentum, and energy), are described in detail by Kozlov *et al.*¹⁶ The results of these simulations are shown in Fig. 6. One can see that in both nanosecond and microsecond-scale array explosions at $r \leq 30\ \mu\text{m}$, one should obtain pressure above $1.2 \times 10^{10}\ \text{Pa}$. Considering the self-similarity²⁶ of the SSW implosion and assuming the azimuthal uniformity of the SSW during the last $15\ \text{ns}$ of convergence, one can expect to obtain pressure larger than $4 \times 10^{10}\ \text{Pa}$ at $r \leq 5\ \mu\text{m}$.

In summary, we carried out research on the convergence of shockwaves generated by both nanosecond and microsecond-scale underwater electrical explosions of cylindrical copper

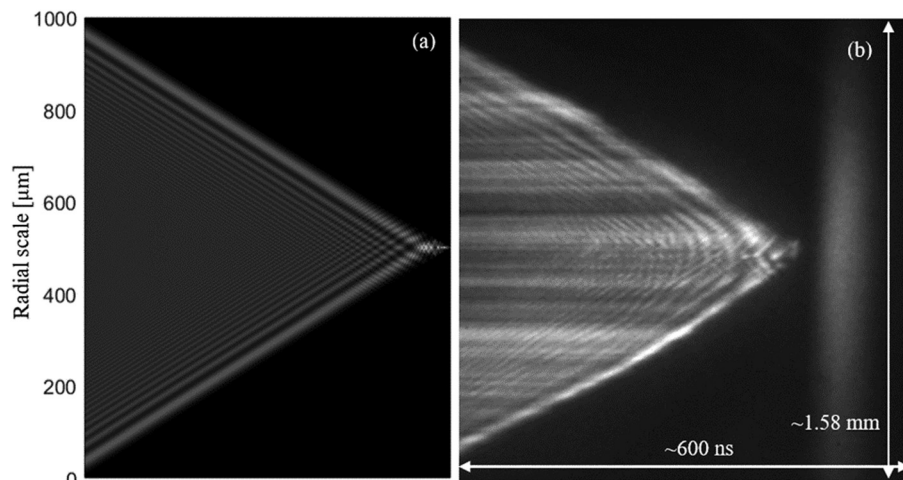


FIG. 5. Time dependent light intensity in the middle of the cylinder obtained by (a) BPM simulation and (b) streak shadowgraph imaging of the converging SSW.

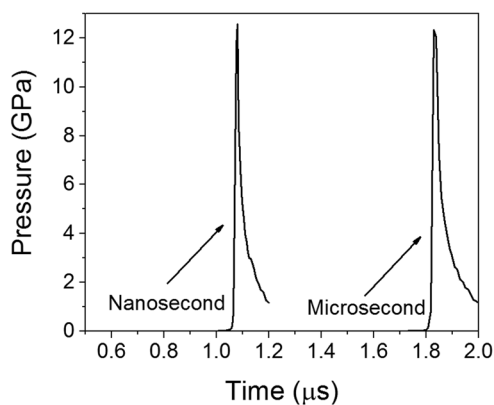


FIG. 6. Pressure at a radius of $30\ \mu\text{m}$ for the nanosecond and microsecond timescales.

wire arrays. Experiments demonstrated that even in the case of an initially azimuthally asymmetric implosion, the SSW self-repairs as it approaches the axis. The interference fringes observed in both framing and streak images of the implosion were found to agree with the results of BPM simulations. The framing shadowgraph images showed the absence of detectable instabilities of the SSW front down to a radius of $30\ \mu\text{m}$. Thus, this research indicated that using a pulsed power generator with a stored energy of only $\sim 500\ \text{J}$, one can produce pressures above $10^{10}\ \text{Pa}$ in the vicinity of the implosion of the SSW. Such a compact and mobile setup can be easily adjusted for the diagnostics of warm dense matter density distribution using either synchrotron radiation or x-ray fluxes produced by powerful lasers.

The authors are grateful to M. Nitishinski and S. Efimov for fruitful discussions and to S. Gleizer for technical assistance.

¹V. E. Fortov, *Extreme States of Matter* (Berlin Heidelberg, Springer-Verlag, 2011).

²P. Renaudin, C. Blancard, J. Clerouin, G. Faussurier, P. Noiret, and V. Recoules, "Aluminum equation-of-state data in the warm dense matter regime," *Phys. Rev. Lett.* **91**, 075002 (2003).

³G. W. Collins, L. B. Da Silva, P. Celliers, D. M. Gold, M. E. Foord, R. J. Wallace, A. Ng, S. V. Weber, K. S. Budil, and R. Cauble, "Measurements of the equation of state of deuterium at the fluid insulator-metal transition," *Science* **281**, 1178 (1998).

⁴G. Huser, M. Koenig, A. Benuzzi-Mounaix, E. Henry, T. Vinci, B. Faral, M. Tomasini, B. Telaro, and D. Batani, "Temperature and melting of laser-shocked iron releasing," *Phys. Plasmas* **12**, 060701 (2005).

⁵E. N. Avrorin, B. K. Vodolaga, V. A. Simonenko, and V. E. Fortov, "Intense shock waves and extreme states of matter," *Phys.-Usp.* **36**, 337 (1993).

⁶M. C. Jones, D. J. Ampleford, M. E. Cuneo, R. Hohlfelder, C. A. Jennings, D. W. Johnson, B. Jones, M. R. Lopez, J. MacArthur, J. A. Mills, T. Preston, G. A. Rochau, M. Savage, D. Spencer, D. B. Sinars, and

J. L. Porter, "X-ray power and yield measurements at the refurbished Z machine," *Rev. Sci. Instrum.* **85**, 083501 (2014).

⁷B. A. Hammel and N. Ignition Campaign Team, "The NIF Ignition Program: Progress and planning," *Plasma Phys. Controlled Fusion* **48**, B497 (2006).

⁸T. R. Boehly, E. Vianello, J. E. Miller, R. S. Craxton, T. J. Collins, V. N. Goncharov, I. V. Igumenshchev, D. D. Meyerhofer, D. G. Hicks, P. M. Celliers, and G. W. Collins, "Shock-timing experiments using double-pulse laser irradiation," *Phys. Plasmas* **13**, 056303 (2006).

⁹A. H. Jones, W. M. Isbell, and C. J. Maiden, "Measurement of the very-high-pressure properties of materials using a light-gas gun," *J. Appl. Phys.* **37**, 3493 (1966).

¹⁰C. L. Morris, N. S. King, K. Kwiatkowski, F. G. Mariam, F. E. Merrill, and A. Saunders, "Charged particle radiography," *Rep. Prog. Phys.* **76**, 046301 (2013).

¹¹S. N. Bland, Y. E. Krasik, D. Yanuka, R. Gardner, J. MacDonald, A. Virozub, S. Efimov, S. Gleizer, and N. Chaturvedi, "Generation of highly symmetric, cylindrically convergent shockwaves in water," *Phys. Plasmas* **24**, 082702 (2017).

¹²D. Yanuka, A. Rososhek, S. Efimov, M. Nitishinskiy, and Y. E. Krasik, "Time-resolved spectroscopy of light emission from plasma generated by a converging strong shock wave in water," *Appl. Phys. Lett.* **109**, 244101 (2016).

¹³O. Antonov, S. Efimov, V. T. Gurovich, D. Yanuka, D. Shafer, and Y. E. Krasik, "Diagnostics of a converging strong shock wave generated by underwater explosion of spherical wire array," *J. Appl. Phys.* **115**, 223303 (2014).

¹⁴O. Antonov, S. Efimov, V. T. Gurovich, V. Bernshtam, and Y. E. Krasik, "Spectroscopy of a plasma formed in the vicinity of implosion of the shock wave generated by underwater electrical explosion of spherical wire array," *Phys. Plasmas* **22**, 053507 (2015).

¹⁵M. Nitishinskiy, S. Efimov, O. Antonov, D. Yanuka, V. T. Gurovich, V. Bernshtam, V. Fisher, and Y. E. Krasik, "Converging shock wave focusing and interaction with a target," *Phys. Plasmas* **23**, 042705 (2016).

¹⁶M. Kozlov, V. T. Gurovich, and Y. E. Krasik, "Stability of imploding shocks generated by underwater electrical explosion of cylindrical wire array," *Phys. Plasmas* **20**, 112701 (2013).

¹⁷J. H. Gardner, D. L. Book, and I. B. Bernstein, "Stability of imploding shocks in the CCW approximation," *J. Fluid Mech.* **114**, 41 (1982).

¹⁸V. Eliasson, M. Kjellander, and N. Apazidis, "Regular versus Mach reflection for converging polygonal shocks," *Shock Waves* **17**, 43 (2007).

¹⁹S. E. Bodner, "Rayleigh-Taylor instability and laser-pellet fusion," *Phys. Rev. Lett.* **33**, 761 (1974).

²⁰G. B. Whitham, *Linear and Nonlinear Waves* (Wiley-Interscience, New York, 1999).

²¹L. Gilburd, S. Efimov, A. Fedotov Gefen, V. T. Gurovich, G. Bazalitski, O. Antonov, and Y. E. Krasik, "Modified wire array underwater electrical explosion," *Laser Part. Beams* **30**(2), 215–224 (2012).

²²A. Fedotov-Gefen, S. Efimov, L. Gilburd, G. Bazalitski, V. T. Gurovich, and Y. E. Krasik, "Generation of a 400 GPa pressure in water using converging strong shock waves," *Phys. Plasmas* **18**, 062701 (2011).

²³A. Grinenko, Y. E. Krasik, S. Efimov, A. Fedotov, V. T. Gurovich, and V. I. Oreshkin, "Nanosecond time scale, high power electrical wire explosion in water," *Phys. Plasmas* **13**, 042701 (2006).

²⁴S. A. Chikovskiy, V. I. Oreshkin, G. A. Mesyats, N. A. Ratakhin, I. M. Datsko, and B. A. Kablambaev, "Electrical explosion of metals in fast-rising megagauss magnetic fields," *Phys. Plasmas* **16**, 042701 (2009).

²⁵K. Okamoto, *Fundamentals of Optical Waveguides* (Academic Press, 2006).

²⁶A. Grinenko, V. T. Gurovich, and Y. E. Krasik, "Implosion in water medium and its possible application for the inertial confinement fusion target ignition," *Phys. Plasmas* **14**, 012701 (2007).